Available online at www.sciencedirect.com

SCIENCE DIRECT

Cement and Concrete Research 35 (2005) 2203 – 2218

Cement and Concrete Research

Modeling of time to corrosion-induced cover cracking in reinforced concrete structures

Kapilesh Bhargava [a,*], A.K. Ghosh [b], Yasuhiro Mori [c], S. Ramanujam [a]

[a] *Architecture and Civil Engineering Division, Bhabha Atomic Research Center, Trombay, Mumbai 400 085, India*
[b] *Health Safety and Environment Group, Bhabha Atomic Research Center, Trombay, Mumbai 400 085, India*
[c] *Associate Professor, Graduate School of Environmental Studies, Nagoya University, Nagoya 464-8603, Japan*

Received 7 June 2005; accepted 7 June 2005

Abstract

Service life of the concrete structures depends on the protective action provided by the cover concrete against the susceptibility of the reinforcement to the corrosive environment. Depending on the level of the oxidation of metallic iron, corrosion products may have much greater volume than the original iron that gets consumed by the process of corrosion. This volume expansion is mainly responsible for exerting the expansive radial pressure at the steel–concrete interface and development of hoop tensile stresses in the surrounding concrete resulting ultimately in the through cracking of the cover concrete. This cover cracking would indicate the loss of the service life for the corrosion-affected structures. In the present paper, an attempt has been made to develop analytical models for predicting the time to cover cracking by considering the residual strength of the cracked concrete and the stiffness provided by the combination of the reinforcement and expansive corrosion products. The problem is modeled as a boundary value problem wherein the governing equations are expressed in terms of the radial displacement and the analytical solutions are presented considering a simple 2-zone model for the cover concrete viz. cracked or uncracked. The analytical models are then evaluated through their ability to reproduce available experimental trends and subsequently a sensitivity analysis has also been carried out to show the influence of the various variable parameters of the proposed models with reference to the experimental trends.

Keywords: Reinforcement corrosion; Modeling; Time to cover cracking; Radial pressure

1. Introduction

One of the most predominant factors responsible for the structural deterioration in concrete structures is identified as corrosion of reinforcement, which may result in damage to the structures in the form of expansion, cracking and eventually spalling of the cover concrete. In addition to this, the structural damage may be due to loss of bond between reinforcement and concrete and loss of reinforcement cross-sectional area; sometimes to the extent that the structural failure becomes inevitable [1]. Therefore, monitoring and control of reinforcement corrosion assume a significant practical importance, if one has to prevent the premature failure of the reinforced concrete structures. Decisions regarding inspection, repair, strengthening, replacement and demolition of the age-degraded reinforced concrete structures are normally affected by the performance of such structures to withstand the extreme events during their service life. The end of service life for the reinforced concrete structures is generally associated with the loss of protective action to be provided by the cover concrete to the reinforcement against the contact with the corrosion inducing agents. Therefore, it would be worthwhile that analytical models be developed to assess the effect of reinforcement corrosion in the reinforced concrete structures, on the structural performance/deterioration for the reasonable prediction of safe residual service life of such structures. The prediction of structural deterioration

* Corresponding author. Tel.: +91 22 25591930; fax: +91 22 25505299.
E-mail address: kapil_66@magnum.barc.ernet.in (K. Bhargava).

0008-8846/$ - see front matter © 2005 Elsevier Ltd. All rights reserved.
doi:10.1016/j.cemconres.2005.06.007

would in turn be very useful to arrive at a cost-effective strategy in handling of the corrosion-affected concrete structures.

In the context of the aforementioned discussion, the prediction of time to cover cracking of reinforced concrete structures may be considered as a useful indicator towards the intensity of the corrosive environment to which the structures are subjected. This would be further useful in estimating the structural capacity to withstand the possible extreme events during the remaining service life of the structures. Prediction of safe residual service life and the time to cover cracking of corroded reinforced concrete structures have been studied by many researchers [2–11]. However, despite these efforts and due to the complexity of the corrosion process itself, some differences between the predicted values and the observed data from the field and laboratory have been reported. This may be attributed to a number of factors viz. the mathematical model for the rate of corrosion process, the residual strength of the concrete once its tensile strength is exceeded and/or the proper estimation of the material properties of the concrete itself besides the mathematical model to describe the structural response.

It is well known that corrosion of reinforcement results in the transformation of metallic iron to the corrosion products due to the process of oxidation resulting in an increase in volume which, depending on the level of oxidation, may be up to about 6.5 times the original iron volume [1,7]. In general the composition of the expansive corrosion products may be expressed as $\{a\cdot Fe(OH)_2 + b\cdot Fe(OH)_3 + c\cdot H_2O\}$ [7], where a, b and c are the variables that depend on the alkalinity of the pore water solution of concrete, the oxygen supply and the moisture content. The different corrosion products will have different volume expansions as presented in Table 1 [1]. This volume increase is believed to be the principal cause of the concrete expansion and ultimately the cover cracking.

In the present paper an attempt is made to formulate a mathematical model for the prediction of time to cracking of the cover concrete in the corroded reinforced concrete structures considering the stiffness offered by reinforcement plus corrosion products combine in addition to the stiffness contribution of concrete. A sensitivity analysis has also been carried out by considering variation of the various parameters of the mathematical model. The model is evaluated through its ability to reproduce the available experimental trends.

Table 1
Correlation between α and α_1 for various corrosion products [1]

Name of corrosion products	FeO	Fe_3O_4	Fe_2O_3	$Fe(OH)_2$	$Fe(OH)_3$	$Fe(OH)_3\cdot 3H_2O$
α	0.777	0.724	0.699	0.622	0.523	0.347
α_1	1.80	2.00	2.20	3.75	4.20	6.40

α = ratio of molecular weight of iron to the molecular weight of the corrosion products.
α_1 = ratio of volume of expansive corrosion products to the volume of iron consumed in the corrosion process.

2. Problem definition for corrosion cracking model

The problem has been modeled as a boundary value problem, wherein to accommodate the expansive corrosion products the internal circular boundary at the steel–concrete interface is displaced resulting in the evolution of the expansive radial pressure at the boundary. Fig. 1(a) shows the initial unrestrained condition for concrete block and reinforcement wherein the reinforcing bar of initial diameter D_i is embedded in the concrete with a clear cover to the reinforcement being C.

A porous zone is assumed to exist around the steel–concrete interface [7] and its thickness is indicated by d_o in Fig. 1(a). The porous zone is assumed to take care of the unevenly distributed voids at the steel–concrete interface which are caused by the various reasons viz. transition from cement paste to steel, entrapped/entrained air voids and corrosion products diffusing into the cement paste capilliary voids, etc. The thickness of the porous zone is the function of the total volume of the voids and in the present paper the same is taken from the reference literature [7] for the purpose of numerical predictions.

Fig. 1(b) shows the free expansion of the corrosion products at the surface of the reinforcement depending on the level of oxidation. Same figure also shows the combined diameter of reinforcement plus corrosion products combine being indicated by D_2 and the reduction in the initial diameter of reinforcement due to corrosion being indicated by $2d_1$.

The surrounding concrete is not subjected to any internal radial pressure during the initial filling of porous zone with rust products; however any further free expansion of corrosion products beyond the porous zone is restrained by the surrounding concrete. At this stage, the surrounding concrete is subjected to an expansive uniform radial pressure p_r and due to which it gets displaced by an amount d_c, i.e. the thickness of the expansive rust products deposited around the reinforcement at the internal boundary as shown in Fig. 1(c). It is noted that in actual practice, since the voids are unevenly distributed at the steel–concrete interface, the filling of voids and the pressure application over the surrounding concrete will be simultaneous and in that case the surrounding concrete will not be subjected to the uniform pressure and this scenario is very difficult to model analytically. Therefore, for the sake of simplicity, the voids around the bar are assumed to be uniform (represented by porous zone) and the pressure application over the surrounding concrete is also assumed to be uniform.

To maintain the equilibrium, the reinforcement plus corrosion products combine would be subjected to an equivalent external pressure p_r as shown in Fig. 1(d). Further increase in the corrosion products results in an

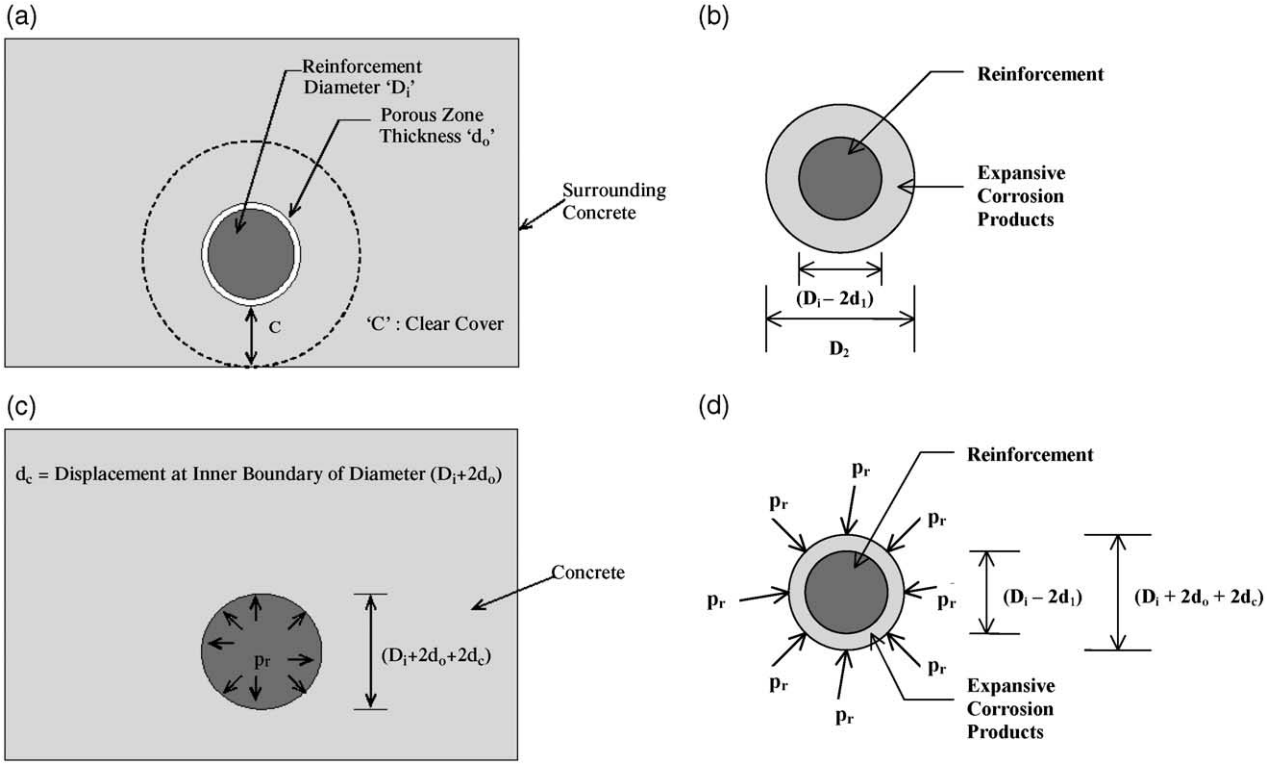

Fig. 1. (a) Initial unrestrained condition for concrete block and reinforcement. (b) Unrestrained condition for reinforcement and expansive corrosion products. (c) Internal radial pressure for concrete block in restrained condition. (d) External pressure for reinforcement plus expansive corrosion products combined.

increase of p_r. Cracking occurs when the maximum hoop stress exceeds the tensile strength f_t of the cover concrete. The cracking begins at the steel–concrete interface and propagates outwards. The concrete is assumed to be a homogeneous, isotropic and linear-elastic material with the inner radius of the thick concrete cylinder being $R_i=(D_i+2d_0)/2$ and the outer radius being $R_o=(R_i+C)$. Initially, the concrete is assumed to be intact and subsequently with the application of the uniform p_r, the propagation of radial splitting cracks will take place in all the directions to the same distance R_c, which is defined as the radius of crack front at which the tensile capacity of the cover concrete is reached. Further progress of corrosion process will result in the development of p_r, which would depend on the residual strength of the cracked concrete and resulting in the further propagation of the crack front or further increase in R_c. The cover concrete is assumed to be fully cracked once R_c becomes equal to R_o.

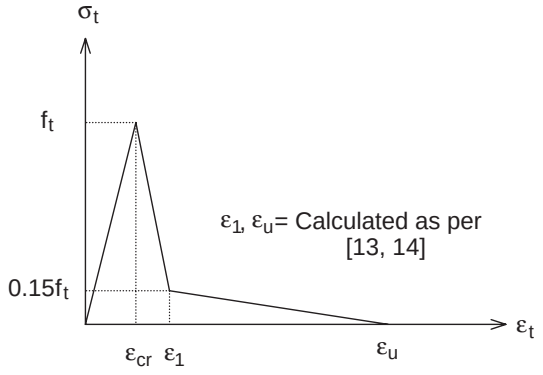

Fig. 2. Idealized stress–strain diagram for cover concrete in uniaxial tension.

In the present study, the strength of the cracked concrete has been considered based on three different assumptions for the development of analytical models: (i) it has strength equal to its original tensile strength, (ii) it does not have any residual strength, and (iii) it has some residual strength which degrades with increasing strain as shown in Fig. 2. The assumption (iii) seems to be the most realistic one. However, analyses based on the first two assumptions would provide some boundary values. Smeared cracking approach is adopted in the formulations and therefore they are presented in terms of the average stresses and strains.

3. Mathematical formulations for the corrosion cracking model

While formulating the corrosion-cracking model, the following basic assumptions are made: (i) although the real problem is practically a three-dimensional one, a two-dimensional approach is proposed for the model for the sake of simplicity and computational efficiency, (ii) corrosion process is spatially uniform around the reinforcement resulting in the spatially uniform buildup of rust products

over the reinforcement thereby resulting in the uniform radial steel–concrete interface pressure due to expansive rust products, (iii) the initiation and rate of corrosion are known in advance, (iv) although the material properties for concrete are time-dependent phenomena, they are considered to be time-independent for the sake of simplicity, (v) mechanical properties pertaining to the corrosion products viz. modulus of elasticity and Poisson's ratio are considered to be same as that of reinforcement, (vi) during the progress of the crack front, no amount of the corrosion products shall be accommodated within the open radial cracks, and (vii) the proposed model is restricted to the stresses resulting from the expansion of corrosion products only.

With reference to Fig. 1, this boundary value problem is modeled and solved as a plane stress problem under radially symmetric conditions, for which the governing stress equilibrium equation is given as follows [12].

$$\frac{d\sigma_r}{dr} + \frac{\sigma_r - \sigma_\theta}{r} = 0 \tag{1}$$

Similarly, the governing strain displacement equations are given as follows.

$$\varepsilon_r = \frac{du}{dr}; \qquad \varepsilon_\theta = \frac{u}{r} \tag{2}$$

where, u=radial displacement at any radius r and the other symbols have their usual meanings.

The stresses are given as follows.

$$\sigma_r = \frac{E_c}{\left(1-\upsilon_c^2\right)}\left(\varepsilon_r + \upsilon_c \varepsilon_\theta\right); \qquad \sigma_\theta = \frac{E_c}{\left(1-\upsilon_c^2\right)}\left(\varepsilon_\theta + \upsilon_c \varepsilon_r\right) \tag{3}$$

where, E_c=modulus of elasticity for cover concrete and υ_c=Poisson's ratio for the cover concrete.

The solution of Eq. (1) using the relations given in Eqs. (2) and (3) will yield the following relations.

$$u = \frac{Ar}{2} + \frac{B}{r} \tag{4}$$

$$\sigma_r = \frac{E_c}{\left(1-\upsilon_c^2\right)}\left[\frac{A}{2}\left(1+\upsilon_c\right) - \frac{B}{r^2}\left(1-\upsilon_c\right)\right] \tag{5a}$$

$$\sigma_\theta = \frac{E_c}{\left(1-\upsilon_c^2\right)}\left[\frac{A}{2}\left(1+\upsilon_c\right) + \frac{B}{r^2}\left(1-\upsilon_c\right)\right] \tag{5b}$$

where, the constants A and B are determined by applying suitable boundary conditions.

In the present study, all the formulations are presented in Appendix A. The formulation in Section A.1 is taken from the reference literature [7], while the formulations given in Sections A.2–A.5 are the present work.

Since corrosion process is a dynamic process and as the rust layer grows thicker, the ionic diffusion distance increases and the rate of rust production decreases because the diffusion is inversely proportional to oxide thickness. Therefore, the growth of rust products may not be taken as a simple linear function based on the steady state corrosion process. The growth of expansive corrosion products is given by the following non-linear function [7].

$$\frac{dW_r}{dt} = \frac{k_p}{W_r} \tag{6}$$

where, k_p is related to rate of metal loss and expressed as follows.

$$k_p = \frac{0.092}{\alpha}\pi D_i i_{cor} \tag{7}$$

where, i_{cor} is the annual mean corrosion rate ($\mu A/cm^2$) and α is the ratio of molecular weight of the iron to the molecular weight of the corrosion products.

Models M1 and M2 presented in Sections A.1 and A.2 are based on the thin-walled concrete cylinder approach and do not consider the effect of crack propagation. The final failure is assumed to occur when the hoop stress σ_θ at R_o becomes equal to the tensile strength of concrete f_t. In both of the models, various considerations pertaining to the rate of rust production, development of internal radial pressure at the steel–concrete interface and cover cracking are similar. However, the model M2 differs from M1 in the sense that it also considers the stiffness offered by reinforcement plus expansive corrosion products combine in addition to the stiffness contribution by the concrete.

Models M3–M5 presented in A.3, A.4 and A.5 are based on the thick-walled concrete cylinder approach and consider the effect of crack propagation. These models also consider the stiffness offered by reinforcement plus expansive corrosion products combine in addition to the stiffness contribution by the concrete. In model M3 the cracked concrete is assumed to maintain the original strength equal to f_t like uncracked concrete, while in model M4 the cracked concrete is assumed to have zero residual tensile strength. However, in actual practice the development of cracks in concrete is a major source of non-linearity and the post-cracking constitutive relations viz. modulus of elasticity etc. depend largely on the fracture energy of concrete which in turn is related to the compressive strength and maximum aggregate size for the concrete among various factors [13]. Therefore, the post-cracking constitutive relations will not remain same as that either for uncracked concrete or corresponding to zero residual tensile strength. Hence, in model M5 it is assumed that the cover concrete maintains some residual tensile strength even after cracking depending on the fracture energy characteristics of the concrete. However, the models M3 and M4 are presented in the paper to reflect the effect of modeling of residual tensile strength of cracked cover concrete and to present the lower and upper bound values for the time to cover cracking. The change in constitutive relations has been considered for the cracked concrete in model M5 and the crack has been considered as smeared crack. Similar approach has also been adopted by other researchers [10].

3.1. Modeling of tensile behaviour of concrete

In the present boundary value problem, hoop and radial directions are the principal directions. The hoop stresses σ_θ are typically tensile in nature while the radial stresses σ_r are typically compressive in nature. It is noted that the tensile failure of concrete is always a discrete phenomenon but, for the sake of simplicity, a smeared crack approach has been used in the present study. Smeared cracks are assumed to form in the radial direction once the principal hoop stresses σ_θ exceed f_t and, therefore, the integration of average hoop tensile strain ϵ_θ over the perimeter would represent the sum of true discrete crack opening [10].

Fig. 2 shows the idealized stress–strain relationship for the cracked concrete used in the present study. Before cracking, the relationship between the average principal tensile stress σ_θ and average principal tensile strain ε_θ is assumed to be linear elastic with a slope equal to E_c, i.e. initial tangent modulus. Once ε_θ exceeds the cracking tensile strain $\varepsilon_{cr}=f_t/E_c$, the cracking in concrete is modeled as a process of tension softening that starts at ε_{cr} and ends at $\varepsilon_\theta=\varepsilon_u$, where ε_u is the strain corresponding to the zero residual tensile strength of concrete. The modulus of elasticity after ε_{cr} depends on the fracture energy G_F of the concrete, which is defined as the energy required to propagate a tensile crack of unit area. The G_F has been calculated as follows [13].

$$G_F = G_{FO}(f_{cm}/f_{cmo})^{0.7} \tag{8}$$

where, f_{cm} is the 28 days cylindrical compressive strength of concrete in MPa; G_{FO} is the base value of fracture energy and depends on the maximum aggregate size for the concrete. In the present study, the G_{FO} has been interpolated for a maximum aggregate size of 20 mm for the experimental study as mentioned in Tables 2 and 4. The f_{cmo} has been taken as 10 MPa [13].

A bilinear softening curve has been used to describe the residual tensile strength of concrete as a function of fictitious crack opening w. The co-ordinates of the fictitious crack opening w_1 corresponding to $\sigma_t=0.15f_t$ and w_u corresponding to $\sigma_t=0$ have been determined as follows [13].

$$w_1 = 2\frac{G_F}{f_t} - 0.15w_u \tag{9}$$

$$w_u = \alpha_F \frac{G_F}{f_t} \tag{10}$$

In the present study, the coefficient α_F has been interpolated for a maximum aggregate size of 20 mm [13] for the experimental study as mentioned in Tables 2 and 4.

Table 2
Experimental data for slab specimen [7]

Specimen designation	D_i (mm)	C (mm)	i_{cor} (μA/cm^2)	f_{cm} (MPa)	f_t (MPa)	E_c (MPa)	υ_c	θ
SPL	16	70	1.79	31.5	3.3	27,000	0.18	2.0

Table 3
Experimental data for type CP specimens [8]

Specimen designation	D_i (mm)	C (mm)	Anode length (mm)	i_{cor} (μA/cm^2)	f_{cm} (MPa)
CPA1 and CPA2	21	27.5	32	100	53
CPB1 and CPB2	21	40.5	42	100	50
CPC1	21	65.5	68	100	53
CPC2	21	65.5	64	100	53
CPD1 and CPD2	21	40.5	42	100	40
CPF1 and CPF2	21	40.5	41	100	53
CPG1	21	40.5	95	100	53
CPG2	21	40.5	42	100	53

For all the specimens E_c and f_t values to be approximated from f_{cm} as given in Reference [15].

It is noted that, due to the presence of coarse aggregate, the use of fracture mechanics model to evaluate the tension softening modulus of the concrete is restricted because of the existence of large fracture process zone (FPZ) also known as width of crack band. As per the available reference literature [14], the thickness of FPZ in different concrete is about 1.5 to 4 times the nominal coarse aggregate size (with the optimum value to be about 3 times the nominal coarse aggregate size). Hence, the size of the specimen should be sufficiently large enough as compared to the FPZ to be justified as a minimum acceptable for a homogeneous continuum modeling. Therefore, in the present study, the smeared strain values ε_1 and ε_u have been calculated based on the characteristic crack-band width h_c consideration to account for the size effect such that $\varepsilon h_c = w$ [14]. Based on the results presented in the reference literature [14], h_c is taken as five times the maximum aggregate size and accordingly the ε_1 and ε_u have been calculated. Similar consideration has also been adopted by other researchers in their analytical predictions [10].

4. Application of proposed models

To assess the performance of proposed models, numerical analyses were carried out for various experimental data as mentioned in Tables 2–4 [7,8,4]. A brief summary of various considerations in the different models is presented in Table 5.

It is an established fact that cracking of cover concrete is governed by a number of factors, e.g. reinforcement diameter, clear cover to reinforcement and uniaxial compressive strength of the concrete. Various material properties

Table 4
Experimental data for beam specimen [4]

Specimen designation	D_i (mm)	C (mm)	i_{cor} (μA/cm^2)	f_{cm} (MPa)	f_t
SPA	16	20	10	30	3.55

The loss in cross-section previous to the application of current was 10.1 μm.

Table 5
Considerations in various models

Consideration ↓		Various models				
		Model 1 (Liu and Weyers, [7])	Model 2 (present work)	Model 3 (present work)	Model 4 (present work)	Model 5 (present work)
Basis of concrete cracking	Thin shell approach	A	A	NA	NA	NA
	Thick shell approach	NA	NA	A	A	A
Number of components	One (only concrete)	A	NA	NA	NA	NA
	Two (concrete and reinforcement plus corrosion products combined)	NA	A	A	A	A
Cracked concrete strength	Zero strength	NA	NA	NA	A	NA
	Full original strength	NA	NA	A	NA	NA
	Appropriate stress–strain relationship, refer to Fig. 2	NA	NA	NA	NA	A
Spatial propagation of radial cracks		NA	NA	A	A	A

A: consideration is applicable and NA: consideration is not applicable.

for the concrete, e.g. modulus of elasticity and tensile strength, are related to uniaxial compressive strength; therefore, their estimation for the cover concrete also assumes significant importance for the accurate evaluation of time to cover cracking. Keeping all these in mind, a sensitivity analysis was also carried out to assess the performance of proposed models while trying to reproduce the available experimental trends. In the proposed sensitivity analysis, the important variables in the proposed models were varied over a wide range about their reference value reported in the reference literature [7]. The following variables were considered for the parametric variation.

i. The effective modulus of elasticity E_{ef} of the cover concrete through variation in the creep coefficient of the cover concrete. The value of creep coefficient θ for the cover concrete has been varied from 0.0 to 3.0.
ii. The tensile strength f_t of the cover concrete has been varied from 0.7 to 4.2 MPa.
iii. The modulus of elasticity E_s of the reinforcement plus corrosion products combine has been varied from 105,000 to 252,000 MPa. The reference value of E_s has been considered as the same value as of reinforcement alone as not much data are reported as far as the material properties of the expansive corrosion products are concerned.
iv. The annual mean corrosion rate i_{cor} has been varied from 0.54 to 26.75 μA/cm^2. The estimation of the parameter k_p depends on i_{cor} and, therefore, the uncertainties in k_p would significantly affect the accurate evaluation of the time to cracking of cover concrete.

The aforementioned parametric study was carried out for the experimental study as mentioned in Table 2 [7]. While carrying out the sensitivity analysis, only one parameter was varied at a time and the other parameters were kept at their reference values as reported in the reference literature [7]. For the experimental study as mentioned in Table 3 [8], the parametric variation was considered only for f_t, which was

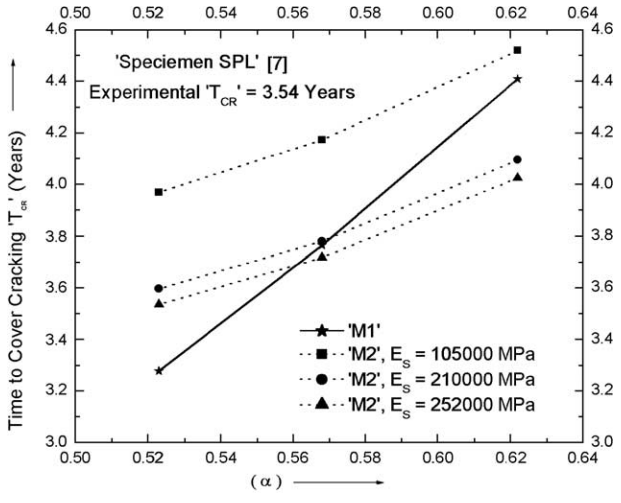

Fig. 3. Time to cover cracking as per models M1 and M2 as a function of α for specimen SPL (Refer Table 2).

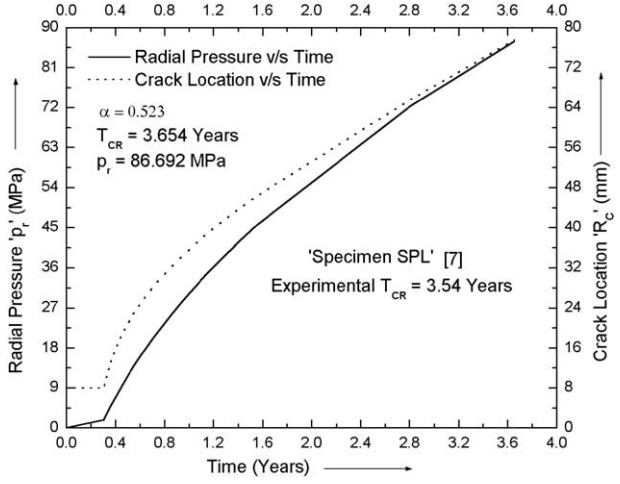

Fig. 4. Radial pressure and crack location as a function of time as per model M3 for specimen SPL (behaviour up to time to cover cracking, refer to Table 2).

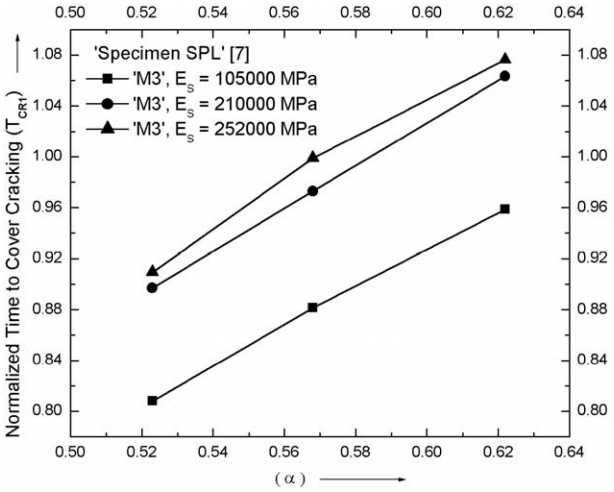

Fig. 5. Normalized time to cover cracking as per model M3 as a function of α for specimen SPL (refer to Table 2).

varied between ranges as defined in available international standard [13].

5. Discussion of results

For the proposed corrosion cracking models, the results of the numerical analyses for the experimental studies as given in Tables 2–4 are presented in Figs. 3–18 and in Tables 6–8.

Fig. 3 demonstrates the variation of time to cover cracking as a function of α for various values of E_s based on M1 and M2 for specimen SPL [7]. For comparison, the experimentally observed value is also presented. M1 and M2 are based on thin cylinder approach and they work well for a limited range of dimensions of the specimen. For larger dimensions, a formulation based on thick cylinder approach (M3) shall be more appropriate. Typical results with M3 are shown in Fig. 4. It is clear from Figs. 3 and 4 that the predicted time to cover cracking as per M2 and M3 is in

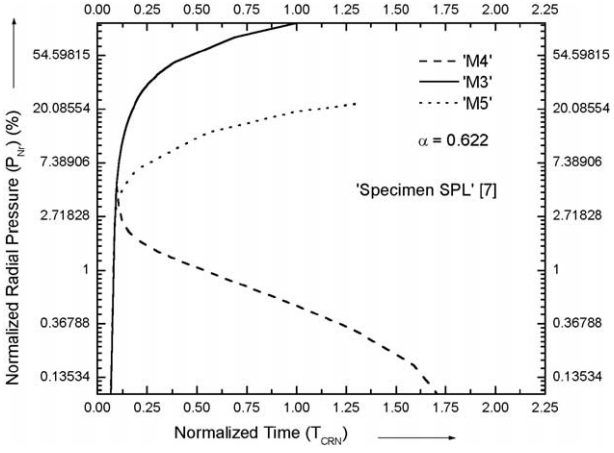

Fig. 6. Normalized radial pressure as a function of normalized time as per models M3–M5 for specimen SPL (behaviour up to time to cover cracking, refer to Table 2).

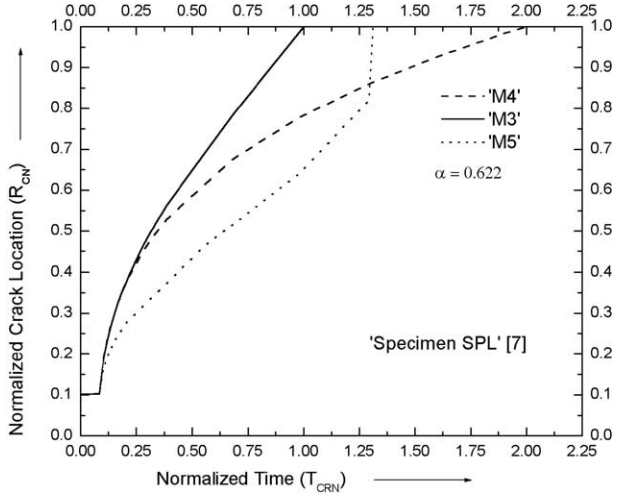

Fig. 7. Normalized crack location as a function of normalized time as per models M3–M5 for specimen SPL (behaviour up to time to cover cracking, refer to Table 2).

good agreement with the experimentally observed time to cover cracking.

To facilitate the presentation of results of various corrosion cracking models in a compact form, normalized parameters are introduced. The results in Figs. 5–10 are presented in normalized forms for specimen SPL as mentioned in Table 2 [7] using the following normalized parameters.

$$T_{CR1} = \frac{\text{Predicted time to cover cracking as per M1 based on thick cylinder approach (years)}}{\text{Predicted time to cover cracking as per M3 (years)}}$$

$$T_{\theta N} = \frac{\text{Predicted time to cover cracking as per M3 or M4 or M5 at any value of } \theta \text{ (years)}}{\text{Predicted time to cover cracking as per M3 at a } \theta \text{ value of 2.0 (years)}}$$

$$T_{CRN} = \frac{\text{Time from initiation of corrosion (years)}}{\text{Predicted time to cover cracking as per M3 (years)}}$$

$$T_{NICOR} = \frac{\text{Predicted time to cover cracking as per M3 or M4 or M5 at any value of } i_{cor} \text{ (years)}}{\text{Predicted time to cover cracking as per M3 (years)}}$$

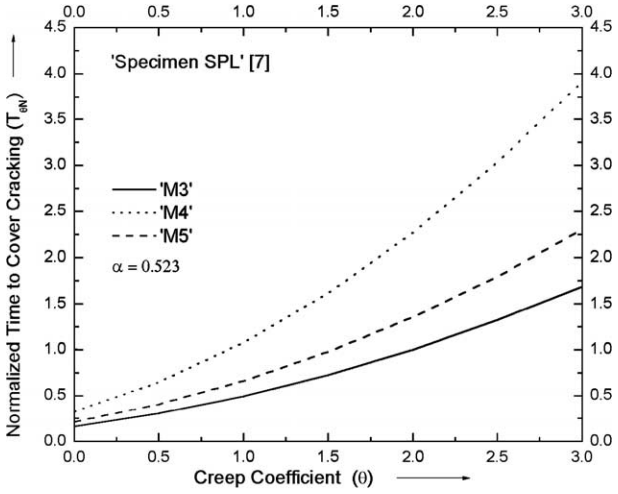

Fig. 8. Normalized time to cover cracking as a function of creep coefficient as per models M3–M5 for specimen SPL (refer to Table 2).

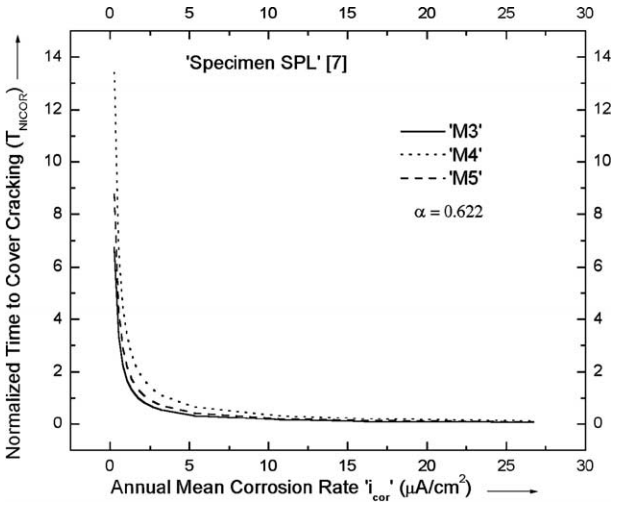

Fig. 9. Normalized time to cover cracking as a function of annual mean corrosion rate as per models M3–M5 for specimen SPL (refer to Table 2).

$$T_{NFT} = \frac{\text{Predicted time to cover cracking as per M3 or M4 or M5 at any value of } f_t \text{ (years)}}{\text{Predicted time to cover cracking as per M3 (years)}}$$

$$P_{Nr} = \frac{\text{Instantaneous radial pressure } P_r \text{ as per M3 or M4 or M5 (MPa)}}{\text{Radial pressure } P_r \text{ as per M3 at the time of cover cracking (MPa)}}$$

$$R_{CN} = \frac{\text{Instantaneous radius of crack front } R_C \text{ as per M3 or M4 or M5 (mm)}}{\text{Outer radius } R_o \text{ of the thick-walled concrete cylinder (mm)}}$$

With these definitions, the range of P_{Nr} and R_{CN} shall be from 0.0 to 1.0. The range of T_{CRN} shall be from 0.0 to 1.0 for M3. This method of normalization facilitates an easy comparison of the results taking the results of M3 as the basis of normalization. In model M3, the cracked concrete is assumed to possess residual strength equal to the original tensile strength of concrete f_t, while in model M4, the cracked concrete is assumed to possess zero residual strength and

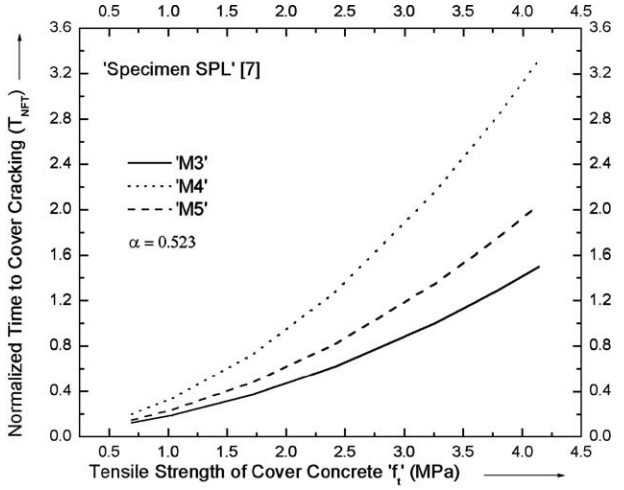

Fig. 10. Normalized time to cover cracking as a function of tensile strength of cover concrete as per models M3–M5 for specimen SPL (refer to Table 2).

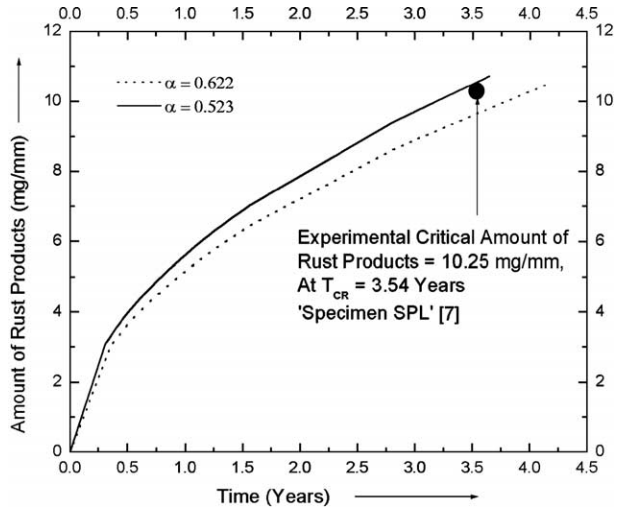

Fig. 11. Amount of rust products as a function of time as per model M3 for specimen SPL (behaviour up to time to cover cracking, refer to Table 2).

therefore these two models will define the lower and upper bound values for T_{CR} and p_r. In model M5, the post-cracking characteristics will neither remain like uncracked concrete nor like concrete with zero residual strength; rather it will depend on the fracture energy characteristics of the concrete and therefore this model will define the intermediate value between the lower and upper bound values for T_{CR} and p_r. Therefore, the normalization of results with reference to the results of model M3 would result in the easy and step-wise understanding of the modeling effects of residual strength of cover concrete.

Fig. 5 presents the normalized predicted time to cover cracking as a function of α in terms of T_{CR1} as per M3 for specimen SPL [7]. It is clear that both the M1 and M3 appear not to show much variation in the prediction of time to cover cracking based on the thick cylinder approach.

It is seen from Figs. 3 and 5 that there appears to be a significant variation in the predicted time to cover cracking

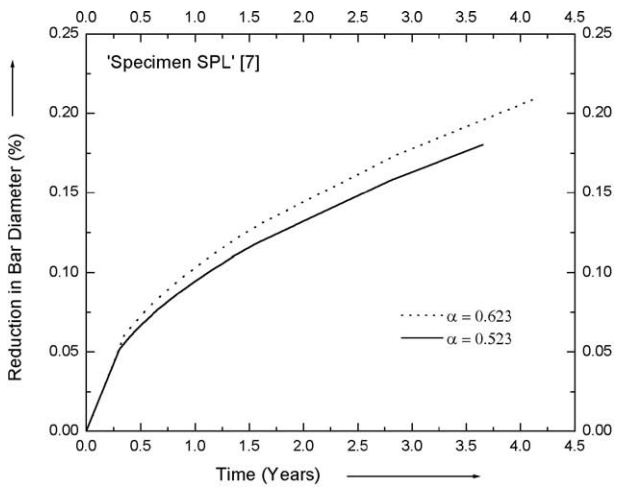

Fig. 12. Reduction in reinforcement bar diameter as a function of time as per model M3 for specimen SPL (behaviour up to time to cover cracking, refer Table 2).

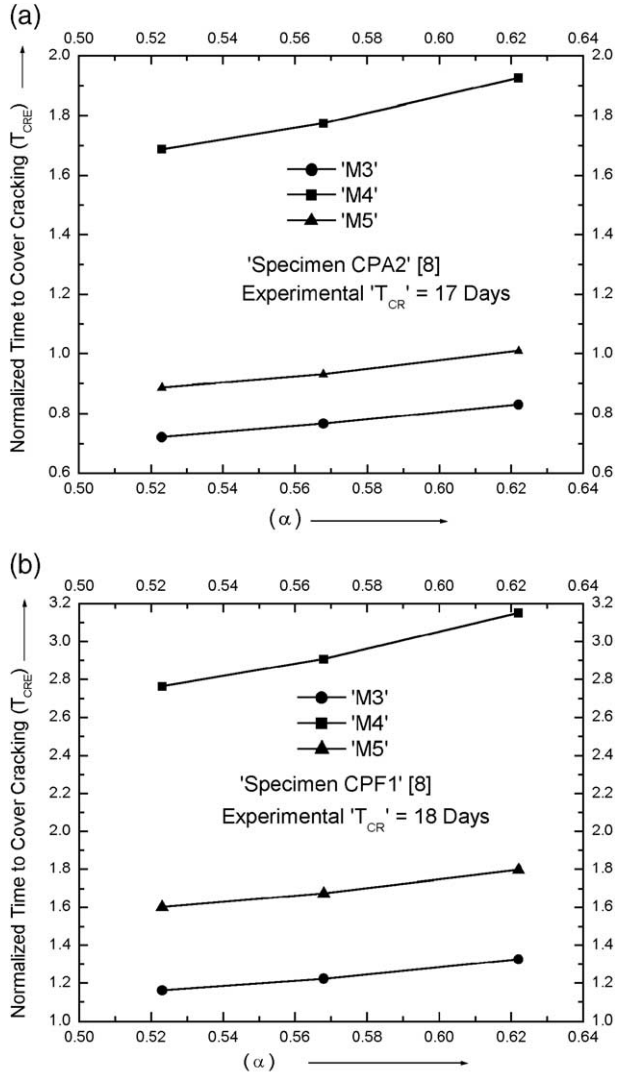

Fig. 13. (a) Normalized time to cover cracking as per models M3–M5 as a function of α for specimen CPA2 (refer to Table 3). (b) Normalized time to cover cracking as per models M3–M5 as a function of α for specimen CPF1 (refer to Table 3).

with the variation in E_s. Lowering the value of E_s would result in a decrease of initial stiffness against the expansion of corrosion products and this would eventually result in the delayed cracking of the cover concrete.

Fig. 6 presents the build-up of p_r at the steel–concrete interface in terms of normalized radial pressure P_{Nr} as a function of normalized time T_{CRN} due to the continued corrosion process as per M3–M5 for specimen SPL [7]. M3 and M5 would result in the increase of p_r with respect to the continued corrosion process till the cover concrete is fully cracked because, in these models, it is assumed that the cracked concrete maintains residual strength, which would result in the increase of the initial stiffness against the expansion of the corrosion products resulting in increased p_r. M4 would result in the decrease of p_r with respect to the continued corrosion process till the cover concrete is fully cracked because, in this model, it is assumed that the cracked concrete does not maintain any residual strength, which would result in the decrease of the initial stiffness against the expansion of the corrosion products resulting in the decreased p_r. It is also evident from the same figure that the value of p_r from M5 is higher than the M4 and lower than the M3. This is because the residual strength of concrete is maximum in case of M3 and minimum in case of M4.

Fig. 7 presents the propagation of crack front from R_i to R_o of thick concrete cylinder in terms of normalized crack location R_{CN} as a function of normalized time T_{CRN} with respect to continued corrosion process as per M3–M5 for specimen SPL [7].

It is clear from Fig. 8 that there appears to be a significant variation in the normalized predicted time to cover cracking $T_{\theta N}$ due to the variation in θ of cover concrete for specimen SPL [7] because variation in θ would result in the variation of E_{ef} and lowering the initial modulus of elasticity for the cover concrete by using higher θ would result in the decrease of

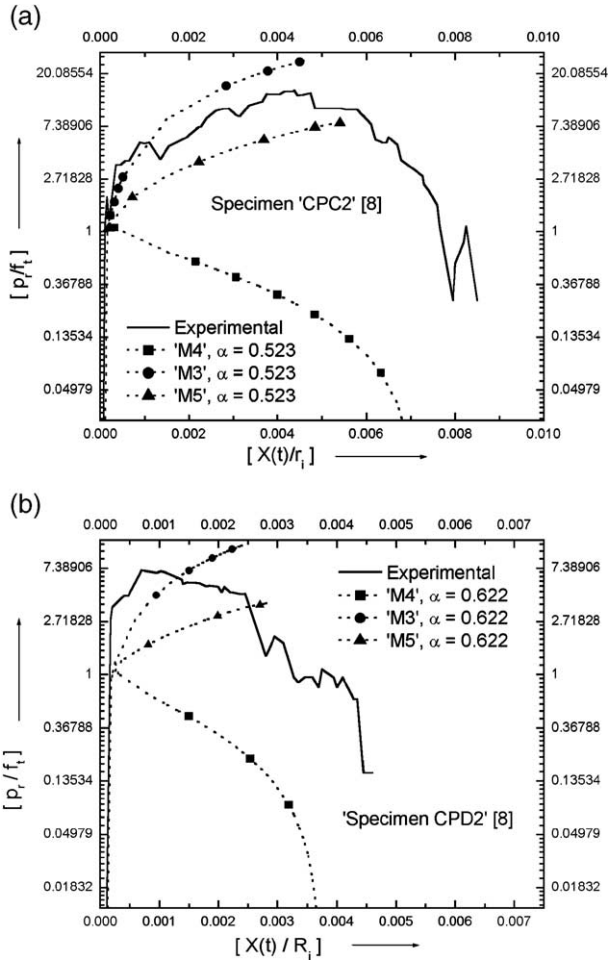

Fig. 14. (a) Relationship between radial pressure-to-tensile strength of cover concrete ratio and corrosion penetration-to-pipe radius ratio for specimen CPC2 (refer to Table 3). (b) Relationship between radial pressure-to-tensile strength of cover concrete ratio and corrosion penetration-to-pipe radius ratio for specimen CPD2 (refer to Table 3).

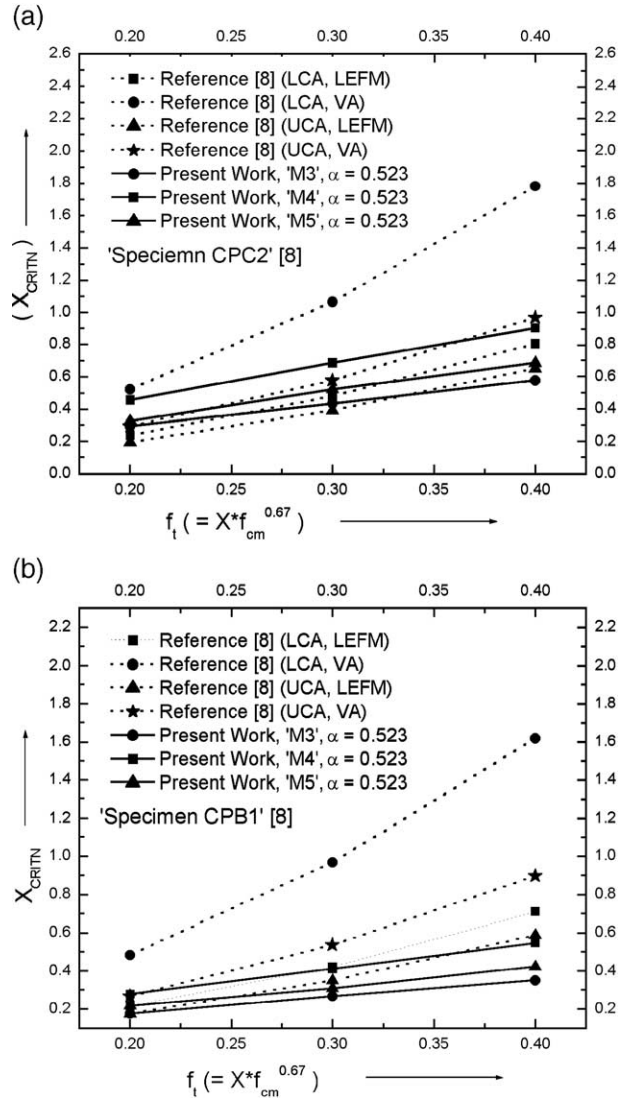

Fig. 15. (a) Normalized corrosion penetration as a function of tensile strength of cover concrete for specimen CPC2 (refer to Table 3). (b) Normalized corrosion penetration as a function of tensile strength of cover concrete for specimen CPB1 (refer to Table 3).

initial stiffness against the expansion of corrosion products resulting in the delayed cracking of the cover concrete.

Fig. 9 presents the influence of i_{cor} on the normalized predicted time to cover cracking T_{NICOR} as per M3–M5 for specimen SPL [7]. Higher i_{cor} would result in the generation of higher amount of the corrosion products for a given period of time resulting in the higher build-up of p_r at the steel–concrete interface and hence the lesser predicted time to cover cracking.

Fig. 10 presents the influence of f_t of cover concrete on the normalized predicted time to cover cracking T_{NFT} as per the M3–M5 for specimen SPL [7]. It is clear that increase in f_t would result in the increase of cracking strain limit ε_{cr} for cover concrete and this would ultimately result in the delayed cracking of the cover concrete.

It is evident from Figs. 5–10 that the predicted time to cover cracking from the M5 is higher than the same from M3

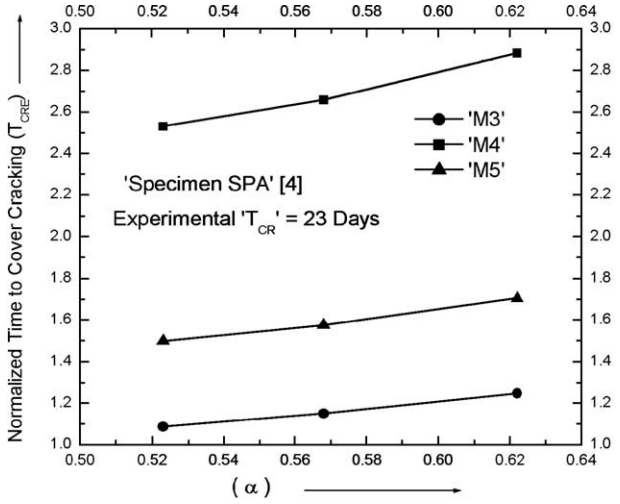

Fig. 16. Normalized time to cover cracking as per models M3–M5 as a function of α for specimen SPA (refer to Table 4).

and lower than that predicted by M4. This is because the stiffness is minimum for M4 and maximum for M3.

Fig. 11 demonstrates the amount of rust products generated per unit length of the bar as a function of time as per M3 for specimen SPL [7]. Fig. 12 shows the reduction in bar diameter expressed in terms of percentage of initial reinforcement diameter as a function of time for different values of α as per M3 for specimen SPL [7]. For comparison, the experimentally observed value at the time of cover cracking is also presented in Fig. 11. It is evident that the predicted values are in good agreement with the experimentally observed value.

The following additional normalized parameters are introduced to facilitate the presentation of results in Figs. 13–18 for other specimens as mentioned in Tables 3 and 4.

$$T_{CRE} = \frac{\text{Predicted time to cover cracking as per M3 or M4 or M5 (years)}}{\text{Experimentally observed time to cover cracking (years)}}$$

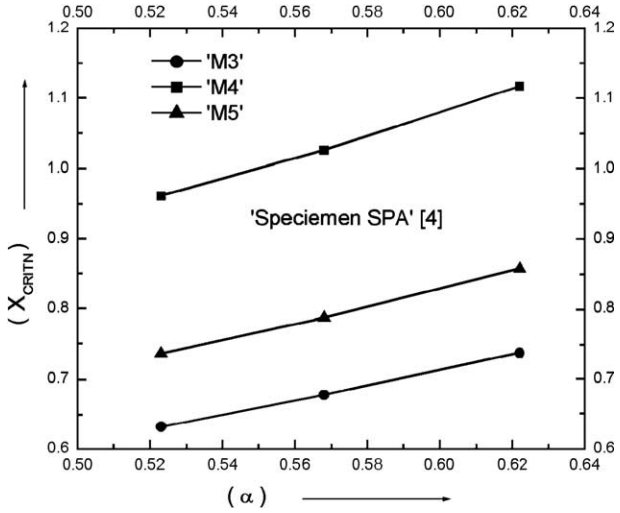

Fig. 17. Normalized corrosion penetration as a function of α for specimen SPA (refer to Table 4).

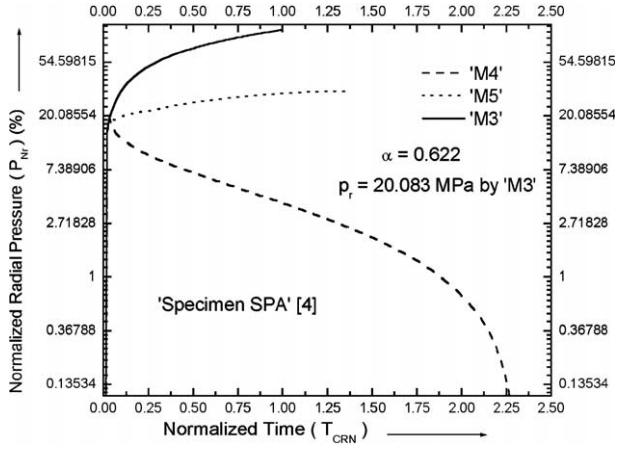

Fig. 18. Normalized radial pressure as a function of normalized time as per models M3–M5 for specimen SPA (behaviour up to time to cover cracking, refer to Table 4).

$$X_{\mathrm{CRITN}} = \frac{\text{Predicted corrosion penetration as per M3 or M4 or M5 (mm)}}{\text{Experimentally observed corrosion penetration (mm)}}$$

Fig. 13(a) and (b) present the variation of normalized time to cover cracking (T_{CRE}) as a function of α based on M3–M5 for specimens CPA2 and CPF1 [8]. For comparison, the experimentally observed values are also presented. It is clear from the figures that the predicted time to cover cracking as per M5 is in good agreement with the experimentally observed time to cover cracking; M3 predicts lower values and M4 predicts higher values than M5, thus defining the lower and upper bound range of the predicted values. The observed trend is similar to the one shown in Figs. 3 and 5 and is attributed to basically the modeling of residual strength of cover concrete in different models. Similar behaviour has also been reported in the analytical predictions of other researchers [7,10].

Table 6 presents the comparison of experimental and predicted values of peak radial pressure-to-tensile strength of cover concrete ratio ($p_{\mathrm{rmax}}/f_{\mathrm{t}}$) for all the specimens mentioned in Table 3 [8]. Analytical predictions have been presented: (i) as per present work using models M3–M5 and (ii) as per reference work [8] considering Localized Corrosion Approach (LCA) and Uniform Corrosion Approach (UCA) by using the appropriate and defined values of cover to anodic length ratio (C/L) in the available empirical equation for p_{rmax} in the reference literature. It is clear from the table that the predicted values as per M5 are in good agreement with the predicted values as per reference work considering UCA, since model M5 is derived considering UCA. Model M3 predicts higher values and model M4 predicts lower values than model M5. The models M3 and M4 are also derived considering UCA; the difference in predicted values with respect to M5 is attributed to the modeling of residual strength of cover concrete.

Fig. 14(a) and (b) present the $p_{\mathrm{r}}/f_{\mathrm{t}}$ as a function of $X(t)/R_{\mathrm{i}}$) as per models M3–M5 for specimens CPC2 and CPD2 [8]. Here $X(t)$ is the corrosion penetration at any time t since initiation and R_{i} is the pipe radius in the reference literature [8]. For comparison, experimentally observed plots are also presented. In model M5, the radial pressure increases with increasing $X(t)/R_{\mathrm{i}}$ and reaches a peak value when R_{c} has propagated to about 90% of the cover; beyond that stage the pressure is maintained and a slight fall is observed when R_{c} reaches to R_{o}. Similar behaviour has also been observed in the analytical prediction of other researchers [10], which also highlights sudden release of pressure followed by the fast decay to zero when R_{c} penetrates the cover. However, present models predict the value of p_{r} required for R_{c} to reach up to R_{o} only. The same behaviour as mentioned above has also been reported in Fig. 6 for specimen SPL [7]. It is also evident from the same figures that the value of $p_{\mathrm{r}}/f_{\mathrm{t}}$ from M5 is higher than the M4 and lower than the M3. This is because the residual strength of concrete is maximum in case of M3 and minimum in case of M4.

Table 6
Comparison of experimental and predicted values of ($p_{\mathrm{rmax}}/f_{\mathrm{t}}$) for type CP specimens as mentioned in Table 3 [8]

Specimen designation	($p_{\mathrm{rmax}}/f_{\mathrm{t}}$)					
	Experimental value	Analytical prediction				
		Reference (Torres-Acosta [8])		Present work, $\alpha=0.523$		
		Localized corrosion approach	Uniform corrosion approach	Model M3	Model M4	Model M5
CPA1	6.32	3.15	2.02	6.06	1.23	2.40
CPA2	4.40			(6.06)	(1.19)	(2.40)
CPB1	4.24	4.83	2.97	11.32	1.31	4.29
CPB2	3.11			(11.32)	(1.26)	(4.28)
CPC1	6.04	7.81	4.80	20.89	1.37	7.91
CPC2	14.56	7.98		(20.89)	(1.32)	(7.90)
CPD1	8.22	4.83	2.97	11.31	1.31	3.85
CPD2	6.96			(11.32)	(1.26)	(3.84)
CPF1	4.94	4.87	2.97	11.32	1.31	4.03
CPF2	2.75			(11.31)	(1.26)	(4.02)
CPG1	4.12	3.84	2.97	11.32	1.31	4.03
CPG2	4.12	4.83		(11.31)	(1.26)	(4.02)

Values inside bracket correspond to $\alpha=0.622$.

Table 7
Comparison of experimental and predicted values of X_{CRIT}/d_a for type CP specimens as mentioned in Table 3 [8]

Specimen designation	X_{CRIT}/d_a							
	Experimental value	Analytical approach						
		Reference (Torres-Acosta [8])				Present work, $\alpha=0.523$		
		Localized corrosion approach		Uniform corrosion approach		Model M3	Model M4	Model M5
		LEFM approach	Volumetric approach	LEFM approach	Volumetric approach			
CPA1	0.0038	0.0035	0.0043	0.0030	0.0025	0.00095 (0.0011)	0.0014 (0.0017)	0.0010 (0.0012)
CPA2	0.0050							
CPB1	0.0097	0.0035	0.0079	0.0029	0.0044	0.0024 (0.0028)	0.0038 (0.0044)	0.0027 (0.0032)
CPB2	0.0076							
CPC1	0.0058	0.0036	0.0079	0.0030	0.0044	0.0037 (0.0043)	0.0058 (0.0068)	0.0044 (0.0051)
CPC2	0.0092	0.0036	0.0080	0.0030	0.0044			
CPD1	0.0028	0.0032	0.0034	0.0026	0.0019	0.0011 (0.0013)	0.0018 (0.0021)	0.0013 (0.0016)
CPD2	0.0036							
CPF1	0.0045	0.0036	0.0056	0.0030	0.0031	0.0017 (0.0020)	0.0026 (0.0030)	0.0019 (0.0022)
CPF2	0.0048							
CPG1	0.0025	0.0033	0.0045	0.0030	0.0031	0.0017 (0.0020)	0.0026 (0.0030)	0.0019 (0.0022)
CPG2	0.0048	0.0036	0.0056	0.0030	0.0031			

Values inside bracket correspond to $\alpha=0.622$.

The difference in plots of analytical predictions and experimental observations is attributed to the following: (i) the analytical models are derived considering UCA while the experiments have been carried out considering localized corrosion; this has resulted in pressure fluctuations indicating stress relaxations due to progressive crack opening and thus highlighting the dependence of p_{rmax} on C/L [8] and (ii) the modeling of post-crack behaviour, i.e., the residual strength of the cracked concrete. Overall, the present models M3–M5 predict reasonably accurate range of p_{rmax}/f_t that are in line with the experimentally observed and analytically predicted values in reference literature [8] and the analytical prediction of other researchers [10].

Table 7 presents the comparison of experimental and predicted values of (X_{CRIT}/d_a) for all the specimens as mentioned in Table 3 [8]. Here X_{CRIT} is the corrosion penetration at cover cracking and d_a is the maximum aggregate size in the reference literature [8]. The analytical predictions have been presented: (i) as per present work using models M3–M5 and (ii) as per reference work [8] by using two approaches namely Linear Elastic Fracture Mechanics (LEFM) and Volumetric Approach (VA) and considering LCA and UCA by using the appropriate and defined values of

Table 8
Effect of f_t on the predicted values of p_{rmax}/f_t for type CP specimens as mentioned in Table 3 [8]

Specimen designation	f_t values (CEB-FIP[13])	Analytical prediction of p_{rmax}/f_t				
		Reference (Torres-Acosta [8])		Present work ($\alpha=0.523$)		
		Localized corrosion approach	Uniform corrosion approach	Model M3	Model M4	Model M5
CPA1	0.2 $(f_{cm})^{0.67}$	3.15	2.02	6.11	1.56	2.67
	0.3 $(f_{cm})^{0.67}$			6.06	1.18	2.17
	0.4 $(f_{cm})^{0.67}$			6.05	1.04	1.73
CPB1	0.2 $(f_{cm})^{0.67}$	4.83	2.97	11.34	1.68	4.85
	0.3 $(f_{cm})^{0.67}$			11.31	1.27	3.99
	0.4 $(f_{cm})^{0.67}$			11.30	1.12	3.33
CPC2	0.2 $(f_{cm})^{0.67}$	7.98	4.80	25.70	1.72	9.40
	0.3 $(f_{cm})^{0.67}$			25.70	1.31	7.68
	0.4 $(f_{cm})^{0.67}$			25.70	1.16	6.37
CPD1	0.2 $(f_{cm})^{0.67}$	4.83	2.97	11.33	1.81	4.79
	0.3 $(f_{cm})^{0.67}$			11.31	1.23	3.25
	0.4 $(f_{cm})^{0.67}$			11.30	1.15	3.09
CPF1	0.2 $(f_{cm})^{0.67}$	4.87	2.97	11.31	1.65	4.72
	0.3 $(f_{cm})^{0.67}$			11.31	1.26	3.58
	0.4 $(f_{cm})^{0.67}$			11.31	1.11	3.00
CPG1	0.2 $(f_{cm})^{0.67}$	3.84	2.97	11.31	1.65	4.72
	0.3 $(f_{cm})^{0.67}$			11.31	1.26	3.58
	0.4 $(f_{cm})^{0.67}$			11.31	1.11	3.00

cover to anodic length ratio (C/L) in the available empirical equations for X_{CRIT} in the reference literature. It is clear from the table that the predicted values as per M5 are in good agreement with the predicted values as per reference work considering UCA since model M5 is derived considering UCA. However, in the reference literature [8], it has been reported that the VA tends to give a closer prediction of the dependence of X_{CRIT} on system dimensions. The models M3 and M4 are also derived considering UCA; the difference in predicted values with respect to M5 is attributed to the modeling of residual strength of cover concrete. The difference in experimental and analytical predictions as per present work is attributed mainly to the effect of localized corrosion thus highlighting the dependence on C/L and the modeling of post-cracking behaviour of cover concrete. It is therefore inferred that the present models M3–M5 predict reasonably accurate range of X_{CRIT}/d_a that are in line with the experimentally observed and analytically predicted values in reference literature [8].

Table 8 presents the effect of tensile strength of concrete on the predicted values of p_{rmax}/f_t for all the specimens as mentioned in Table 3 [8]. Similarly, Fig. 15(a) and (b) present the effect of tensile strength of concrete on the normalized corrosion penetration X_{CRITN} for specimens CPC2 and CPB1 [8]. It is noted that various relationships have been reported in the different international standards [13,15,16] for the evaluation of f_t of the concrete, thus resulting in different values of f_t even for the same value of the f_{cm} for the concrete. Therefore, to examine the performance of the model and for the purpose of parametric study, f_t has been evaluated using different formulations given in the available international standard [13] in addition to the one defined in the reference literature [8]. It is clear from Table 8 that increase in f_t would result in the increase in absolute value of p_{rmax}; however, the ratio p_{rmax}/f_t may result in the opposite trend. Similarly, the increase in f_t would also result in the increase in X_{CRITN} as evident in Fig. 15(a) and (b). Increase in f_t would result in the increase of cracking strain limit ε_{cr} for cover concrete and this would in turn result in the delayed cracking of the cover concrete, increase in p_{rmax} and increase in X_{CRIT}. Similar trends have also been reported in the analytical predictions of other researchers [7,10].

Figs. 16–18 present the analytical predictions for the specimen SPA as mentioned in Table 4 [4]. It is clear from Figs. 16 and 17 that the predicted values of T_{CRE} and X_{CRITN} are in good agreement with the experimentally observed values. The analytically predicted trends are in line with the other reported analytical trends [7,10]. The analytical trend observed in Fig. 18 is similar to the one observed in Figs. 6 and 14.

It is clear from the present study that the cover cracking is also dependent on the type of corrosion products because different corrosion products would have different volume expansion on formation and thus have different mass densities. However, in the present study, the values of the predicted times to cover cracking are reported for two values of α viz. 0.523 and 0.622 and normally these two represent the lower and upper bounds in case of the reinforcement corrosion under chloride environment. Therefore, the actual cover cracking time would lie between these two bounds.

6. Conclusions

The following conclusions can be drawn from the present study.

The proposed models M2–M5 consider the stiffness offered by the reinforcement plus corrosion products combine, which is an improvement over available mathematical models [3–5,7,10]. The growth of rust products has been incorporated as a non-linear function, which is again an improvement over the steady state linear function available in some of the earlier mathematical models [3–5]. Model M5 also considers the process of tension softening in the cover concrete once the principal hoop strain exceeds the value of cracking tensile strain and this is an improvement over available mathematical models [3–5,7].

Correlation with the available experimental data [4,7,8] shows that the presented models M2–M5 are mathematically quite simple, capable of reproducing the experimental trends and providing the reasonable estimates of the predicted time to cover cracking. These models are also capable of predicting the peak value of radial steel–concrete interface pressure and the corrosion penetration at cover cracking, which are again in line with the analytically predicted and experimentally observed values as reported in reference literature [8]. M3 and M4 predict the lower and upper bounding values of T_{CR} and p_r. This is because the residual strength of concrete is maximum in the case of M3 and minimum in the case of M4. In M5, the residual strength depends on the fracture energy characteristics of the concrete and therefore this model will define the intermediate value between the lower and upper bound values for T_{CR} and p_r.

The results of the numerical analyses show that the predicted time to cover cracking is significantly affected by the types of corrosion products, corrosion rate and the selection of the material properties for the cover concrete namely E_c and f_t, which is in line with the analytical predictions of other researchers [7,10]. It is also clear from the sensitivity analysis that predicted time to cover cracking is affected significantly by the modulus of elasticity E_s of the reinforcement plus corrosion products combine in addition to the aforementioned factors.

The process of tension softening in the cover concrete, once the principal hoop strain exceeds the value of cracking tensile strain as considered in M5, does have a significant effect over the predicted time to cover cracking, radial steel–concrete interface pressure and corrosion penetration at cover cracking, which are again in line with the analytical trends reported by other researchers [8,10].

Model M2 is based on thin cylinder approach and an improvement over model M1 as it considers the stiffness

offered by reinforcement. Models M3–M5 are based on thick cylinder approach and also include the stiffness offered by reinforcement. These models differ from one another in the manner in which the residual strength of the cracked concrete is modeled. In the present framework of modeling, M5 would be the most realistic one.

Appendix A

A.1. Model 1 (M1) [7]

In this formulation, the solution of Eq. (4) is obtained by specifying $u=d_c$ at $r=R_i$ and $\sigma_r=0$ at $r=R_o$. The radial stress at the inner boundary is given as $\sigma_r=-p_r$. Where, p_r is the radial pressure at the concrete/rust products interface. For the cover concrete to be fully cracked, p_r shall be evaluated based on the condition that the minimum stress required to cause cracking of cover concrete equals f_t of concrete, considering the cover C to be very thin. The radial stress equilibrium at the inner boundary would result in d_c.

For a constant corrosion rate, the integration of Eq. (6) would give time to cover cracking TCR (in years) as follows.

$$T_{CR}=\frac{W_{crit}^2}{2k_p} \tag{A-1}$$

where W_{crit} is the critical mass of the corrosion products (mg/mm) needed to induce cracking of cover concrete.

A.2. Model 2 (M2)

In this formulation, the following boundary conditions shall be applied for the solution of Eqs. (4) (5a) (5b).

For concrete:

$$u=d_c \quad \text{at} \quad r=R_i \quad \text{and} \quad \sigma_r=0 \quad \text{at} \quad r=R_o. \tag{A-2a}$$

For the combination of reinforcement and corrosion products:

$$\sigma_r=-p_r \quad \text{at} \quad r=R_i \quad \text{and}$$
$$u=\{D_2-(D_i+2d_o+2d_c)\}/2 \quad \text{at} \quad r=D_2/2. \tag{A-2b}$$

This would result in the following relationship for p_r.

$$p_r=\frac{2E_{ef}d_c}{(D_i+2d_o)\left(\frac{R_o^2+R_i^2}{R_o^2-R_i^2}+\upsilon_c\right)} \tag{A-3}$$

where, E_{ef} is the effective modulus of elasticity of the cover concrete and given as follows.

$$E_{ef}=\frac{E_c}{1.0+\theta} \tag{A-4}$$

where, θ is the creep coefficient for the cover concrete. For cover concrete to be fully cracked, the principal hoop stress σ_θ shall be equal to f_t at outer boundary. For very thin cover, this condition would result in the following relationship for p_r.

$$p_r=\frac{Cf_t}{R_i} \tag{A-5}$$

In the model M1, the radial displacement of concrete at $r=R_i$ is equal to the thickness of the rust layer d_c beyond the porous zone. However, in this model, the radial displacement at the inner boundary shall be evaluated from continuity of displacement at $r=R_i$ besides the rust products since the stiffness of concrete as well as the combination of the reinforcement and the corrosion products are concerned. This condition would result in the following relationship for d_c.

$$d_c=\frac{D_2-2R_i}{2+\left\{\frac{E_{ef}(1.0-\upsilon_s)}{E_s\left(\frac{R_o^2+R_i^2}{R_o^2-R_i^i}+\upsilon_c\right)}\right\}\left(\frac{D_2}{R_i}\right)} \tag{A-6}$$

where, E_s and υ_s are the effective modulus of elasticity and Poisson's ratio for the reinforcement plus expansive corrosion products combine. In the present study, the stiffness contribution from expansive corrosion products is not modeled separately to keep the model simple and more amenable to analytical solution. Considering the corrosion products explicitly would also require the data regarding its modulus of elasticity and Poisson's ratio, which are not readily available.

The solution of Eqs. (A-3) (A-5) and (A-6) would result in the estimation of D_2. The mass of the expansive corrosion products per unit length of the reinforcement W_r is obtained as follows.

$$W_r=\frac{\pi}{4}\rho_r\alpha_1\left[\frac{D_2^2-D_i^2}{\alpha_1-1.0}\right] \tag{A-7}$$

where, ρ_r is the mass density of the corrosion products and is defined as follows.

$$\rho_r=\frac{\rho_s}{\alpha\alpha_1} \tag{A-8}$$

where, ρ_s is the mass density of reinforcing steel and α_1 is the volume expansion ratio for the expansive corrosion products. Once W_r equals the critical value, the time to cover cracking then shall be evaluated by Eq. (A-1).

A.3. Model 3 (M3)

This model is based on thick-walled cylinder approach and considers the propagation of radial splitting cracks from R_i to R_o. A schematic representation of the cover concrete into two zones of cracked and uncracked concrete is shown in Fig. 19. Cracked concrete is represented as 'zone 1' between the reinforcement plus expansive corrosion pro-

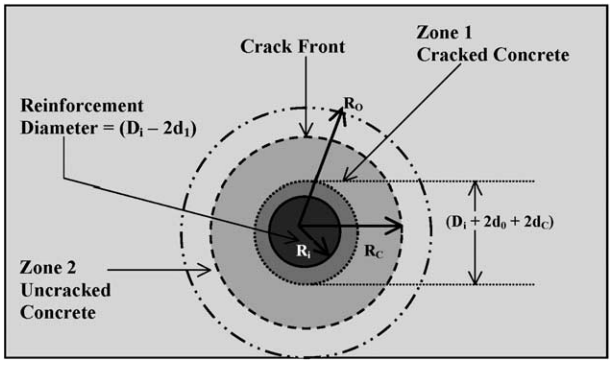

Fig. 19. Two zones for cover concrete due to corrosion cracking process.

ducts combine and R_c, while the uncracked concrete is represented as 'zone 2' between R_c and R_o. At R_c, the principal hoop stress σ_θ becomes equal to f_t of the cover concrete. The cover concrete is assumed to be fully cracked when R_c becomes equal to R_o. It is further assumed that the cover concrete maintains the original strength equal to its tensile capacity in 'zone 1' and, therefore, the modulus of elasticity remains unchanged.

In this formulation, Eq. (4) and Eqs. (5a) and (5b) shall be considered separately for both 'zone 1' and 'zone 2' of the cover concrete and the solution, which shall be obtained by applying the boundary conditions as defined by Eqs. (A-2a) and (A-2b). Eqs. (6) (7) and (A-7), would give W_r and D_2 at any time t from initiation of corrosion. Eq. (A-6) would give d_c; R_c at time t is given by the following relationship.

$$R_c = \sqrt{\frac{p_r R_i^2 R_o^2}{\left(f_t R_o^2 - f_t R_i^2 - p_r R_i^2\right)}} \tag{A-9}$$

When R_c becomes equal to R_o, the cover is assumed to be fully cracked.

A.4. Model 4 (M4)

This model is similar to the formulation M3 but differs from it in the sense that the cracked concrete is assumed to have zero residual strength, i.e., the inner boundary of the structural concrete is shifted from R_i to R_c. In this formulation, too, Eq. (4) and Eqs. (5a) and (5b) shall be considered separately for both 'zone 1' and 'zone 2' of the cover concrete and the solution shall be obtained by applying the boundary conditions as defined by Eqs. (A-2a) and (A-2b). Hence, if R_c is to be displaced by d_c then the material between R_i and R_c will have to move by an amount d_{c1} for preserving the volume. Here, d_{c1} is defined as follows.

$$d_{c1} = \frac{R_i}{R_c} d_c \tag{A-10}$$

Following the procedure mentioned for the formulation M3 and making use of Eq. (A-11), d_c is obtained as follows.

$$d_c = \frac{D_2 - 2R_i}{\left[\frac{D_2}{R_c}\left\{\frac{E_{ef}(1.0-\upsilon_s)}{E_s\left(\frac{R_o^2+R_i^2}{R_o^2-R_i^2}+\upsilon_c\right)}\right\}+\frac{2R}{R_i}\right]} \tag{A-11}$$

After the evaluation of d_c, R_c at any instant of time t from initiation of corrosion is defined by Eq. (A-9).

A.5. Model 5 (M5)

This model is also similar to the formulations M3 and M4 but differs from them in the sense that the cracked concrete is assumed to maintain some residual strength after the principal tensile strain in the hoop direction exceeds the cracking tensile strain value of ε_{cr} and therefore the cracking in the cover concrete is modeled as a process of tension softening, as shown in Fig. 2. Similar behaviour of the concrete has also been considered by other researchers [10]. However, the present work develops a simple analytical solution instead of a finite difference-based solution presented in the reference literature [10] by considering a 2-zone model of concrete (cracked and uncracked) as shown in Fig. 19. The modulus of elasticity for the 'zone 1' concrete is defined by the secant slope of the descending branches of the stress–strain curve as shown in Fig. 2 and the modulus of elasticity for the 'zone 2' concrete is defined by its original value.

In this formulation, too, Eq. (4) and Eqs. (5a) and (5b) shall be considered separately for both 'zone 1' and 'zone 2' of the cover concrete and the solution shall be obtained by applying the boundary conditions as defined by Eqs. (A-2a) and (A-2b). In addition to this, at R_c, radial stresses due to 'zone 1' and 'zone 2' concretes are equal. These conditions would result in the following relationships.

$$u_c = d_c \frac{E_{ef1}\left[(1-\upsilon_{c2})R_c^2+(1+\upsilon_{c2})R_o^2\right]\left[2R_iR_c\right]}{E_{ef1}\left[(1-\upsilon_{c2})R_c^2+(1+\upsilon_{c2})R_o^2\right]\left[(1+\upsilon_{c1})R_c^2+(1-\upsilon_{c1})R_i^2\right]-E_{ef2}\left(R_c^2-R_i^2\right)\left(R_c^2-R_o^2\right)\left(1-\upsilon_{c1}^2\right)} \tag{A-12}$$

where, u_c is the radial displacement at R_c. The subscripts 1 and 2 to the various symbols will carry the usual meanings of the symbols for 'zone 1' and 'zone 2' concrete, respectively. The p_r and R_c are defined as follows.

$$p_r = \frac{E_{ef1}}{\left(1-\upsilon_{c1}^2\right)}\left[\left\{\frac{u_cR_c - d_cR_i}{R_c^2-R_i^2}\right\}(1+\upsilon_{c1}) - \frac{R_c}{R_i}\left\{\frac{d_cR_c-u_cR_i}{R_c^2-R_i^2}\right\}(1-\upsilon_{c1})\right] \tag{A-13}$$

$$R_c = \sqrt{\frac{1}{\left[\frac{f_t(1+\upsilon_{c2})}{E_{ef2}C_k}-\frac{1}{R_o^2}\right]}} \tag{A-14}$$

where, C_k is given as follows.

$$C_k = \frac{(1+\upsilon_{c2})u_c R_c R_o^2}{(1+\upsilon_{c2})R_o^2 + (1-\upsilon_{c2})R_c^2} \quad \text{(A-15)}$$

For an assumed value of R_c, Eq. (A-14) would give C_k. After the evaluation of C_k, Eq. (A-15) would give u_c. After getting the value of u_c, d_c shall be evaluated from Eq. (A-12). Then, by using Eq. (A-13), p_r at the reinforcement–concrete interface can be estimated. Then Eq. (A-6) would result in D_2. The solution of Eqs. ((A-7), (7) and (A-1)) would result in the time required for the crack to reach at the location R_c.

References

[1] P.K. Mehta, P.J.M. Monteiro, Concrete Microstructure, Properties and Materials, 1st edition, Indian Concrete Institute, Chennai, 1997.

[2] P.D. Cady, R.E. Weyers, Deterioration rates of concrete bridge decks, J. Transp. Eng. 110 (1) (1984) 34–45.

[3] Z.P. Bazant, Physical model for steel corrosion in sea structures—applications, J. Struct. Div., ASCE 105 (6) (1979) 1155–1166.

[4] C. Andrade, C. Alonso, F.J. Molina, Cover cracking as a function of rebar corrosion: Part I. Experimental test, J. Mat. Struct. 26 (1993) 453–464.

[5] S. Morinaga, Prediction of Service Lives of Reinforced Concrete Buildings Based on the Rate of Corrosion of Reinforcing Steel, Special Report of the Institute of Technology, Shimizu Corporation, JAPAN, 1989.

[6] B. Martin-Perez, Service Life Modeling of RC Highway Structures Exposed to Chlorides, PhD Dissertation, Dept. of Civil Engineering, University of Toronto, Toronto, 1998.

[7] Y. Liu, R.E. Weyers, Modelling the time-to-corrosion cracking in chloride contaminated reinforced concrete structures, ACI Mat. J. 95 (6) (1998) 675–681.

[8] A.A. Torres-Acosta, Cracking Induced By Localized Corrosion of Reinforcement in Chloride Contaminated Concrete, PhD Dissertation, Dept. of Civil and Environmental Engineering, University of South Florida, Tampa, Florida, 1999.

[9] A.A. Torres-Acosta, A.A. Sagues, Concrete cover cracking with localized corrosion of reinforcing steel, in: V.M. Malhotra (Ed.), Proc. 5th CONMAT/ACI Int. Conf. on Durability of Concrete, SP-192, American Concrete Institute, Farmington Hills, Michigan, 2000, pp. 591–611.

[10] S. Pantazopoulou, K.D. Papoulia, Modeling cover-cracking due to reinforcement corrosion in RC structures, J. Struct. Div., ASCE 127 (4) (2001) 342–351.

[11] Andres A. Torres-Acosta, M. Martinez-Madrid, Residual life of corroding reinforced concrete structures in marine environment, J. Mater. Civ. Eng., ASCE 15 (4) (2003) 344–353.

[12] S.P. Timoshenko, J.N. Goodier, Theory of Elasticity, 3rd edition, McGraw-Hill Book Company, New York, 1970.

[13] CEB-FIP, Comite Euro-International du Beton-Federation International de la Precontrainte - Design Code, Thomas Telford, London, 1990.

[14] Z.P. Bazant, B.H. Oh, Crack-band theory for fracture of concrete, J. Mat. Struct. 16 (1983) 155–177.

[15] ACI 318, Standard Code Requirements for Reinforced Concrete and Commentary, American Concrete Institute, Detroit, 1985.

[16] IS 456, Indian Standard Code of Practice for Plain and Reinforced Concrete, 4th Revision, Bureau of Indian Standards, New Delhi, 2000.